




# Finding Optimal Placement of the Almost Spherical Parallel Mechanism in the Recupera-Reha Lower Extremity Exoskeleton for Enhanced Workspace

Ibrahim Tijjani<sup>(✉)</sup> 

Robotics Innovation Center, German Research Center for Artificial Intelligence (DFKI GmbH), Robert-Hooke-Str. 1, 28359 Bremen, Germany  
ibrahim.tijjani@dfki.de

**Abstract.** The ankle joint of an exoskeleton plays a vital role in maintaining balance and posture during locomotion by grounding the upper body's weight. Parallel designs are advantageous for constructing ankle joints in exoskeleton but challenges include complex workspace analysis and finding the optimal placement in the overall structure of the exoskeleton. This paper presents a strategy for finding the optimal placement of the prototype Active Ankle 3[R2[US]] mechanism in the Recupera-Reha lower extremity exoskeleton for enhanced workspace. To this end, rotative inverse geometric model of the Active Ankle is exploited to find the alignment between principle human joint axes and axes along which the range of motion is optimum. It is demonstrated that by rotating the mechanism along the adduction-abduction axis and by selecting appropriate ball and socket joints, it is possible to enhance the usable workspace of the mechanism for the human wearing the exoskeleton.

**Keywords:** Spherical-parallel manipulators · Kinematic analysis · Optimal placement point · Exoskeletons and prosthesis devices

## 1 Introduction

There has been an increasing societal need for procuring modular ankle exoskeleton devices for medical rehabilitation, walking assistance, and augmenting locomotion strength for the physically disabled, aged persons, and athletes. A parallel manipulator (PM) is a robot system design that offers high stiffness, payload capacity, speed, and accuracy due to combination of two or more kinematic chains. In particular, spherical parallel manipulator (SPM) is a PM which allows only rotational motions of its end-effector platform. For instance, the prominent three (3) degree of freedom (DoF) Agile Eye [3] is a type of SPM and finds application in camera orienting devices. The PKAnkle [11] is a redesigned prototype of Agile Eye that fits in for ankle neuro-rehabilitation and it's capable of providing wide ankle motion ranges but has problems associated to alignment with the

human ankle joint complex. Majority of the researchers in the exoskeleton application domain for gait rehabilitation [1, 2, 4, 10, 12, 14, 16], exploits the advantages of an SPM design approach (see [8] for a recent survey), with emphasis on increasing the workspace, and finding suitable alignment configuration with the human ankle joint.

The novel Active Ankle (see Fig. 1) first introduced in [12] is a wearable ankle exoskeleton device that exploits the advantages of a PM. It is an almost spherical parallel mechanism (ASPM) similar to the SPM in structural design, with a 3 DoF and 3 actuators capable of three principal movements; dorsiflexion-plantarflexion (DF-PF), eversion-inversion (EV-IN), and adduction-abduction (AD-AB) motions. The design of the Active Ankle mechanism represents a module for the ankle and hip joints shown in Fig. 2 of the Recupera-Reha full-body exoskeleton [9] in Fig. 3. An extensive kinematic analysis of the mechanism is available in [5–7]. The current mounting of the active ankle mechanism in the Recupera-Reha exoskeleton has some limitations. The orientation of its joint axes is not properly aligned with that of the human ankle joint complex which leads to a reduced workspace. Hence, it is essential to find an optimal placement point of the ankle mechanism in the exoskeleton leg design. Another challenge with the device is a passive ball and socket joint limit on the motor actuator that leads to a small usable workspace available for the movement trajectories if it's to be utilized, as a use-case for dynamic walking or gait rehabilitation, proper alignment with the human ankle joint complex with increased motion ranges is necessary.

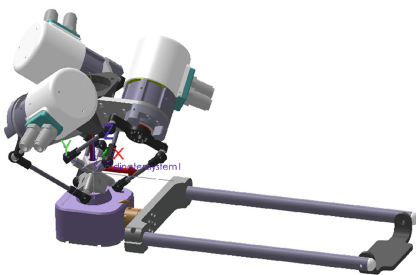


Fig. 1. Active ankle

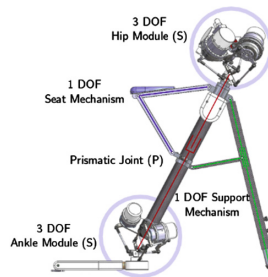


Fig. 2. Joints module

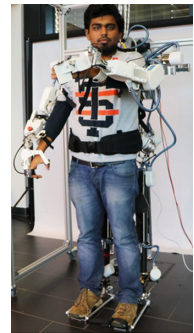


Fig. 3. Full-body exoskeleton [9].

*Contribution.* Since the desire to lift the upper body's weight and perform some dynamic walking with the active ankle mechanism, this paper has exploited the rotative inverse geometric model (RIGM) to produce a larger usable workspace and found an optimal placement configuration point for the ASPM ankle joint which fits better to the human ankle joint complex. Further, a proof that by modifying the opening angle of the ball and socket joints, it is possible to further extend the workspace without making any big structural changes in the system design.

## 2 Rotative Inverse Geometric Model of the ASPM Ankle

This section highlights the analysis of the inverse kinematic problem of the active ankle mechanism adapted from [6]. As earlier stated, the device has a feature of an ASPM, designed to drive a spatial quadrilateral that intersects its three rotative actuators perpendicularly at its end-effector (EE) point. The opening angle of the ball and socket joint for the mechanism is limited by  $\pm 25^\circ$  motor angle constraint ( $q_{min}, q_{max}$ ), while the available range of motion (RoM) for the task space angles ( $\theta_{min}, \theta_{max}$ ), is constrained by a  $\pm 90^\circ$  physical limit ( $\theta$ ). The fascinating feature in the mechanism design structure is that the physical configuration of its joint axes is capable of bearing any force applied without external torque from the motor actuators. In essence, a design structure of the joint axes different from the previous configuration will require additional torques from the motors to drive the device, thus, increased cost. Due to the ASPM design nature of the device, the existence of translation shifts in the EE point is neglected due to its small value when the mechanism is used in the application point of view. Hence, only the rotative universal joints with the spherical cut-joints were utilized in the mechanical design structure, but in the analytical kinematic formulation, the translation shifts were included. The forward kinematic problem that gives the position of the EE as a function of its joint variables is difficult to compute analytically for a complex PM like the ankle joint since it has a limited usable workspace. Therefore, you can not ascertain the feasible workspace that fits into a specific joint configuration. For example, the available workspace in the rotative domain shown in Fig. 4 as reported in the previous variant of the active ankle mechanism. We can not discern which one within the available workspace has the exact configuration for the given set of joint angles. Hence, the knowledge of the positional coordinates of the device alone is not sufficient to determine the placement of the mechanism in the leg. Therefore, we exploit the RIGM that computes the rotative joint space angles and EE positional shifts from the desired orientation, similar to the human ankle joint. However, to achieve a desired orientation of the EE-frame, the RIGM uses the parameterized orientation of the principal movement joint axes vectors represented by  $u_x$ ,  $u_y$  and  $u_z$  instead of the position coordinates to find the input joint angles. The joint axes vectors are obtained from a computer-aided design (CAD) model of the active ankle device and adapted to the RIGM.

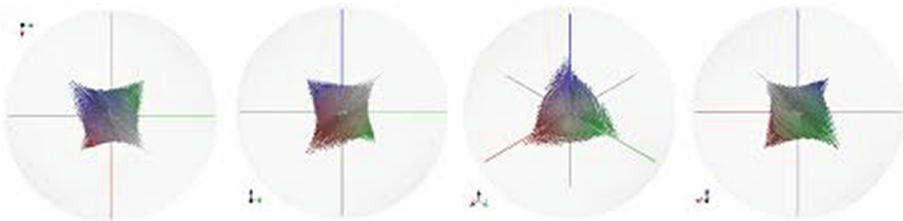


Fig. 4. Feasible workspace configurations adapted in [6].

To find an optimal placement point of the ankle mechanism in the leg, with a similar orientation to the human ankle joint complex in Fig. 5, three different coordinate frame systems were considered at the EE point shown in Fig. 6. The first coordinate frame is the EE-frame (joint axes encoded in yellow color) with a different orientation, a second coordinate frame is the task-space frame located at the EE-point whose joint axes vectors ( $u_x, u_y, u_z$ ) are parallel to the global coordinate frame attached to the leg mount point. Basically, the constraint that mounting frames at the leg mount point and the EE-point should be parallel is the initial choice of optimizing the placement angle ( $\alpha$ ). The third coordinate frame (joint axes encoded in black color) is called the rotated frame. Considering the rotated frame with the joint axes ( $du_x, du_y, du_z$ ) at zero-configuration, only the  $du_z$  joint vector is fixed in the same direction with the z-axis (blue color) of the global frame, unlike  $du_x$  and  $du_y$  which are perpendicular to each other. The ASPM mechanism placement angle  $\alpha$  is the angle between the joint vectors of the task-space frame and the rotated frame. We want to parameterize the rotated frame with respect to the task-space frame and map the generated joint angles which are within the actuator motor limit to the EE-frame.

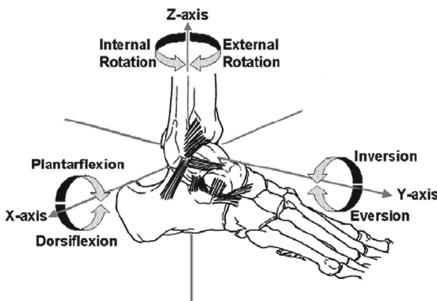


Fig. 5. Human ankle complex [15]

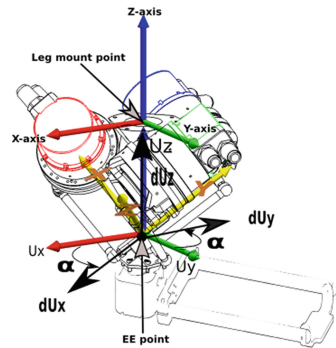


Fig. 6. ASPM ankle frames

The following Table 1 presents the RoM for the movement trajectories. In comparison with the human ankle joint motions reported in [6]. At zero-configuration, you can discern the differences between the human ankle motion ranges and the three other mechanisms from their absolute (Abs.) sum of the minimum (Min.) and maximum (Max.) angles. The active ankle has limited RoM in the DF-PF motion of the previous work [6], which is an essential motion trajectory for the ankle joint. However, this could be insufficient for dynamic walking towards rehabilitation of gait. SPKM and PKAnkle devices have limited RoM in their respective EV-IN and AD-AB motion types, which could be sufficient motion range for human normal daily walking activities. However, for stair ascending and descending, a minimum RoM of 37° and 56° respectively is required according to the authors in [13] for the DF-PF motion trajectory, producing an absolute sum of 93°. Therefore, an increased RoM is imperative for enhanced dynamic walking for the most frequent human daily activities.

**Table 1.** Comparison between human and existing ankle joint mechanisms RoM.

Motion type	Human ankle			Active ankle [6]			SPKM [1]			PKAnkle [11]		
	Min.	Max.	Abs.	Min.	Max.	Abs.	Min.	Max.	Abs.	Min.	Max.	Abs.
DF-PF	-20°	50°	70°	-19.83°	37.23°	57.06°	29.8°	45.8°	75.6°	-40°	35°	75°
EV-IN	-15°	35°	50°	-15.00°	35.00°	50.00°	17°	22°	39°	-25°	20°	45°
AD-AB	-30°	45°	75°	-29.20°	36.96°	66.16°	25.9°	36°	69.10°	-20°	10°	30°

### 3 Optimal Placement of the ASPM Ankle in the Leg

It is of interest to know the criteria for modification of the current design even though the results obtained from the kinematic model analysis of the mechanism in [6] demonstrated the DoFs for the three rotative actuators with a workspace modality that shows three principal motion trajectories for application as an ankle joint. However, for use-case as an ankle rehabilitation device towards enhancing dynamic walking, the following two cases could be used to increase the usable workspace for the active ankle:

1. **Case 1:** Increasing the opening angle for the ball and socket joint to have wider RoM.
2. **Case 2:** For the optimal placement point of the mechanism in the leg, we require the transformation of the task space frame respecting the rotated frame.

#### 3.1 Parameterization Procedure

Matlab simulation is used to improve the RoM for the ASPM ankle joint. A total number of 1000 samples ( $n$ ) for a time ( $t$ ) range from 0 to 1 with a sampling rate of 0.001 is used for the simulation. The  $\pm 25^\circ$  motor angle constraints are initially set for the simulation to compare the previous experimental results obtained in [6] and later increased to  $\pm 27^\circ$ . The parameterization procedure is described in Algorithm 1, for a range of  $\alpha$  in Line 1 which is limited by  $\theta$ , the transformation matrix (T) in Line 2 is built from a Matlab command *makehgtform*, that rotates the vector  $u_z$  by  $\alpha$  in radians. Then, Line 3 extracts the rotation matrix (R) part of T. The vectors  $u_x$  and  $u_y$  are now parameterized by R in Line 4 and Line 5 respectively as the orientation vectors, such that they are orthogonal to each other and lie on the same plane perpendicular to the  $u_z$ . The *RIGM* function in Line 6 takes into account the computed orientation vectors from the parameterized vectors, and the motor constraints as input while Line 7 produces the joint space angles which are within the motor constraints as outputs.

In Algorithm 2, the function routine *TaskSpaceAngles* in Line 1 of Algorithm 2 maps out the joint space angles to  $\alpha$  in Lines 2, 3, and 4 respectively, to find the relationship between them. Line 7 returns the boundary limits on the task space angle curves computed from Lines 5 and 6. The function routine

*IntersectCurves* in Line 8 uses the Mathworks *InternX* function to compute the minimum and maximum intersection points on the three curves. The intersection points within the curves that are less than or greater than zero are computed in Line 9 and Line 10 respectively. These are the trade-off points within the actuator motor limit and the physical limit.

---

**Algorithm 1:** Parameterization procedure

---

**Input:** Joint axes vectors:  
 $\vec{u}_x = [-0.8165; 0.4082; 0.4082]$ ,  
 $\vec{u}_y = [0; -0.7071; 0.7071]$ , and  
 $\vec{u}_z = [1; 1; 1]$

**Output:** Joint angles:  
 $q_x, q_y,$  and  $q_z$

```

1 for  $\alpha = -\pi : 2\frac{\pi}{n} : \pi$ ; do
2    $\mathbf{T} \leftarrow \begin{bmatrix} -0.3333 & 0.6667 & 0.6667 & 0 \\ 0.6667 & -0.3333 & 0.6667 & 0 \\ 0.6667 & 0.6667 & -0.3333 & 0 \\ 0 & 0 & 0 & 1 \end{bmatrix}$ ;
3    $\mathbf{R} \leftarrow \mathbf{T}(1 : 3, 1 : 3)$ ;
4    $du_x \leftarrow (\mathbf{R} \cdot \vec{u}_x)$ ;
5    $du_y \leftarrow (\mathbf{R} \cdot \vec{u}_y)$ ;
6   Function RIGM( $du_x,$ 
    $du_y, q_{min}, q_{max}$ ):
7      $[q_x, q_y, q_z] \leftarrow (-25^\circ \leq$ 
    $q \leq 25^\circ)$ ;
8     return  $q_x, q_y, q_z$ 
9 End
```

---



---

**Algorithm 2:** Computation of task space angles

---

**Input:**  $(\alpha, q_{min}, q_{max}, q_x, q_y, q_z)$   
**Output:** Task space angles  
 $(\theta_{min}, \theta_{max})$

```

1 Function
  TaskSpaceAngles( $\alpha, q_x, q_y, q_z, q_{min}, q_{max}$ ):
2    $L_x \leftarrow [\alpha; q'_x]$ 
3    $L_y \leftarrow [\alpha; q'_y]$ 
4    $L_z \leftarrow [\alpha; q'_z]$ 
5    $L_{min} \leftarrow$ 
    $[\alpha; q_{min} \cdot length(\alpha)]$ 
6    $L_{max} \leftarrow$ 
    $[\alpha; q_{max} \cdot length(\alpha)]$ 
7   return  $L_{min}, L_{max}$ 
8   Function
  IntersectCurves( $L_{min},$ 
    $L_{max}, L_x, L_y, L_z$ ):
9      $\theta_{min} \leftarrow max(\theta < 0)$ 
10     $\theta_{max} \leftarrow min(\theta > 0)$ 
11    return  $\theta_{min}, \theta_{max}$ 
12 End Function
```

---

## 4 Simulation Result

The Matlab simulation in Fig. 7 shows the graphical plot of the  $(\theta_{min}, \theta_{max})$  in (radian) against  $(q_x, q_y,$  and  $q_z)$  also in (radian) that are limited by the same motor constraints. The graph describes the computation of the intersection points on the rotated curves. The upper and lower horizontal lines (maximum and minimum) and the vertical lines are created to show all the intersection points, the point with the highest RoM closer to the zero-configuration is selected as the optimal placement point of the mechanism in the leg. The graphical representation for the variation of  $(\theta_{min}, \theta_{max})$  and  $\alpha$ , respecting the  $\pm 25^\circ$  motor constraint on the ball and socket joint opening angle is depicted in Fig. 8, for  $0^\circ$  configuration point. The sum of the intersection points on the lower and upper boundaries of each curve produced the absolute sum of  $63.46^\circ$  DF-PF,  $74.35^\circ$  EV-IN, and  $71.29^\circ$  AD-AB RoM for the three principal motion trajectories of the ASPM ankle module. However, modifying the opening angle of the ball and socket joint which is constrained by a motor constraint of  $\pm 27^\circ$ , the result in Table 2 is obtained for the following configuration points ( $0^\circ, \pm 15.12^\circ, \pm 30.24^\circ, 45^\circ$ ). The green shaded part is the chosen optimal placement point of the ankle

mechanism in the leg. We can see a symmetric movement in both directions for the chosen point producing a wide RoM for the motion trajectories.

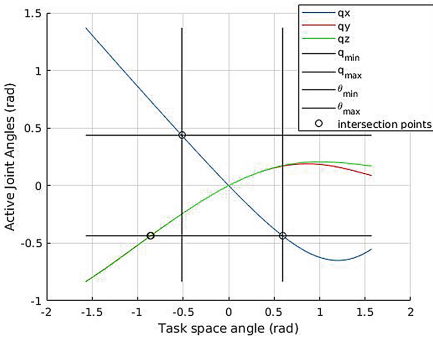


Fig. 7. Intersection points on the curves

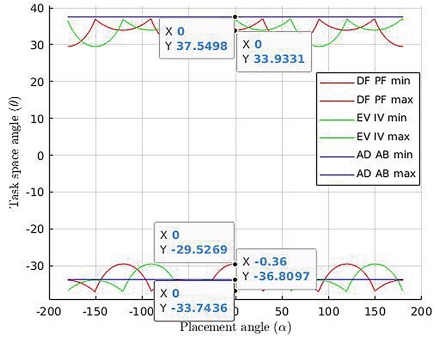


Fig. 8. 0° configuration point

Table 2. Ankle Motion Ranges with  $\pm 27^\circ$  motor constraint.

Placement angle( $\alpha$ )	DF-PF			EV-IN			AD-AB		
	Min.	Max.	Absolute	Min.	Max.	Absolute	Min.	Max.	Absolute
0°	-31.83	37.28	69.11	-39.77	40.14	79.91	-33.74	40.26	74
-15.12°	-33.74	37.87	71.61	-38.16	33.61	71.77	-33.74	40.26	74
15.12°	-33.74	37.85	71.59	-33.74	37.85	71.59	-33.74	40.26	74
-30.24°	-39.94	40.26	80.20	-37.28	31.83	69.11	-33.74	40.26	74
30.24°	-40.09	40.26	80.35	-31.83	37.28	69.11	-33.74	40.26	74
45°	-37.86	33.41	71.27	-33.64	38.17	71.81	-33.74	40.26	74

## 5 Conclusion

This paper presents the optimal placement of the ASPM ankle joint in the leg. The previous prototype has an opening angle on the ball and socket joints that leads to the motor constraint of  $\pm 25^\circ$ , limiting the workspace of the mechanism principal movement trajectories. Likewise, there is difficulty finding an optimal placement point for the mechanism in the leg. However, employing the RIGM to the mechanism, an optimal placement point was obtainable with an enhanced workspace for the motion ranges. Since the ASPM ankle represents a module for the ankle and hip joint, only the ankle joint module is presented in this work with an increased opening angle of the ball and socket joints to  $\pm 27^\circ$ . Forthwith, a large workspace was produced at 30.24° configuration point. As a prospect for the future, the dynamic model of the ASPM ankle joint will be used to control the device and enhance dynamic walking towards rehabilitation of gait, as a proof of concept to the Recupera-Reha full-body exoskeleton.

**Acknowledgement.** This research work is conducted at the Robotics Innovation Center, DFKI GmbH, Bremen, Germany in the M-RoCK project funded by the Federal Ministry of Education and Research with grant no. 01IW21002. Additionally, the author acknowledges the support of the Nigerian-German Academic Exchange Programme, sponsored by the DAAD.

## References

1. Bi, Z.M.: Design of a spherical parallel kinematic machine for ankle rehabilitation. *Adv. Robot.* **27**(2), 121–132 (2013)
2. Gallardo-Alvarado, J., Rodriguez-Castro, R., Perez-Gonzalez, L., Aguilar-Najera, C.R.: Kinematics of the 3(RPSP)-S fully spherical parallel manipulator by means of screw theory. *Robotics* **7**(2), 29 (2018). <https://doi.org/10.3390/robotics7020029>
3. Gosselin, C., St.-Pierre, É., Gagné, J.A.M.: On the development of the agile eye. *IEEE Robot. Autom. Mag.* **3**(4), 29–37 (1996). <https://doi.org/10.1109/100.556480>
4. Kirchner, E.A., et al.: Recupera-Reha: Exoskeleton technology with integrated biosignal analysis for sensorimotor rehabilitation (2016)
5. Kumar, S., Bongardt, B., Simnofske, M., Kirchner, F.: Task space controller for the novel active ankle mechanism (2016). <https://doi.org/10.13140/RG.2.2.30022.11845>
6. Kumar, S., Bongardt, B., Simnofske, M., Kirchner, F.: Design and kinematic analysis of the novel almost spherical parallel mechanism active ankle. *J. Intell. Robot. Syst.* **94**, 303–325 (2019)
7. Kumar, S., Nayak, A., Bongardt, B., Mueller, A., Kirchner, F.: Kinematic analysis of active ankle using computational algebraic geometry. In: Zeghloul, S., Romdhane, L., Laribi, M.A. (eds.) *Computational Kinematics*. MMS, vol. 50, pp. 117–125. Springer, Cham (2018). [https://doi.org/10.1007/978-3-319-60867-9\\_14](https://doi.org/10.1007/978-3-319-60867-9_14)
8. Kumar, S., Wöhrle, H., de Gea Fernández, J., Müller, A., Kirchner, F.: A survey on modularity and distributivity in series-parallel hybrid robots **68**, 102–367 (2020). <https://doi.org/10.1016/j.mechatronics.2020.102367>. ISSN: 0957-4158
9. Kumar, S., et al.: Modular design and decentralized control of the Recupera exoskeleton for stroke rehabilitation. *Appl. Sci.* **9**(4), 626 (2019)
10. Leiyu, Z., et al.: Design and workspace analysis of a parallel ankle rehabilitation robot (PARR). *J. Healthcare Eng.* **2019**, 1–10 (2019). <https://doi.org/10.1155/2019/4164790>
11. Malosio, M., Negri, S., Pedrocchi, N., Vicentini, F., Caimmi, M., Molinari Tosatti, L.: A spherical parallel 3 degrees-of-freedom robot for ankle-foot neuro-rehabilitation. In: *IEEE Engineering in Medicine and Biology Society Conference*, pp. 3356–3359 (2012)
12. Marc, S., Shivesh, K., Bertold, B., Frank, K.: Active ankle - an almost-spherical parallel mechanism. In: *Proceedings of ISR 2016: 47st International Symposium on Robotics*, pp. 1–6 (2016)
13. Stauffer, R.N., Chao, E.Y., Brewster, R.C.: Force and motion analysis of the normal, diseased, and prosthetic ankle joint, vol. 127, pp. 189–196 (1977)



14. Wang, C., Fang, Y., Guo, S., Chen, Y.: Design and kinematical performance analysis of a 3-RUS/RRR redundantly actuated parallel mechanism for ankle rehabilitation. *J. Mech. Robot.* **5**(4), 041003 (2013). <https://doi.org/10.1115/1.4024736>
15. Yuki, T.: Effect of arch supports on ankle-subtalar complex instability: a biomechanical experimental study. *Foot Ankle Int.* **24**(8), 634–639 (2003). <https://doi.org/10.1177/107110070302400811>
16. Zuo, S., Li, J., Dong, M., Zhou, X., Fan, W., Kong, Y.: Design and performance evaluation of a novel wearable parallel mechanism for ankle rehabilitation. *Front. Neurorobotics* **14**, 9 (2020). <https://doi.org/10.3389/fnbot.2020.00009>